JOURNAL OF MATERIALS SCIENCE **34** (1999) 2807–2812

Preparation of tin oxide gels with versatile pore structures

NAE-LIH WU, S-YEN WANG
Department of Chemical Engineering, National Taiwan University, Taipei, Taiwan, Republic of China
E-mail: nlw001@ccms.ntu.edu.tw

Hydrous tin oxide gels were subjected to consecutive solvent-evaporation (SE) and CO_2 supercritical (CS) drying steps, followed by re-hydration at low (30%) humidity, and the effects on pore structure of the SE drying duration and particle surface potential of the gel were investigated. The difference in surface potential has been found to impose significant variations in initial pore size distribution, while the SE drying step tends to narrow such differences and simultaneously reduce the mean pore size. It is demonstrated that varieties of pore structures have thus been obtained by simply varying these two parameters.

1. Introduction

Tin oxide (SnO_2) is a material that has many technological applications. It has been used, for instance, as catalysts for oxidation of organics [1–3], solid-state gas detectors [4–6], transparent conductive glasses and heat mirrors [7, 8]. Each of these applications prefers certain pore structure characteristics for optimum performance. In the cases of catalysis and sensor applications, for instance, large pores along with a high specific surface area are generally preferable. Large pores impose less resistance to molecular diffusion and hence may alleviate diffusion-limitation kinetics as well as accelerate the response dynamics for chemical sensors. A higher specific surface area, on the other hand, can give a higher overall catalytic activity and sensor sensitivity, respectively. Optoelectronic applications prefer uniform pore size distribution (PSD) with minimum amount of pores that have a diameter greater than the visible-light wavelength, so as to maintain high transparency.

Sol-gel process has proven to be an attractive method for large-scale commercial fabrication of tin oxide monoliths, films and powders [9–14]. When the hydrous tin oxide gel thus prepared is subjected to the conventional solvent-evaporation (SE) drying process, the resulted dry gel contains predominantly pores with a diameter less than 2 nm (micro-pores). Being insensitive to the gel-processing conditions, including aging time and temperature and solution pH value [9–14], the pore structure is known to result mainly from the capillary-force effect [15]. We, on the other hand, have also conducted detailed study on the shrinking behavior of tin oxide gel in CO_2 supercritical (CS) drying [16]. The gels shrink extensively during the solvent-exchanging steps and the shrinking behaviors have been shown to be a strong function of several processing parameters, particularly the surface potential of the constituent particles within the gels. Different pore-contraction behaviors from that in SE drying are anticipated based on the established gel-shrinking mechanisms therein. In an attempt to gain a greater flexibility in tailoring the pore structure, experiments were thus carried out to subject the hydrous gels to hybrid drying processes which combine the SE and CS drying steps. We reported in this work the pore structures resulting from a drying protocol consisting of consecutive SE + CS drying steps, followed by re-hydration at low (30%) humidity. In brief, varieties of pore structures which differ greatly in PSD and total pore volume have been obtained by varying the surface potential of the constituent particles of the hydrous gel and the duration of the SE drying step.

2. Experimental

Hydrous tin oxide gels were prepared by a spontaneous solution-sol-gel method [12, 13], which is summarized in Fig. 1. An aqua-alcoholic (H_2O/ethanol = 3 : 2 by volume) solution containing 0.03 M $SnCl_4 \cdot 5\ H_2O$ was aged at room temperature. Solution-to-sol and sol-to-gel transitions took place spontaneously to produce gelatinous precipitates. Once the precipitate sedimented, the supernatant solution was decanted and fresh water was replenished. These procedures were repeated until the solution pH value reached ~4.0. The precipitate was then collected in a Teflon container and was either directly subjected to the CS drying or first partially SE-dried at 34 °C under 75% relative humidity to produce a free-standing gel (Fig. 1). These gels will hereafter be referred to as the *acidic gels*. In other cases, ammonia was added into the solution containing the precipitate to give a pH of ~9.0 and the white precipitate became completely peptized within 24 h into a transparent sol (Fig. 1). Free-standing *basic gels* were obtained by subjecting the sols to the SE pre-drying under the same conditions as the acidic ones.

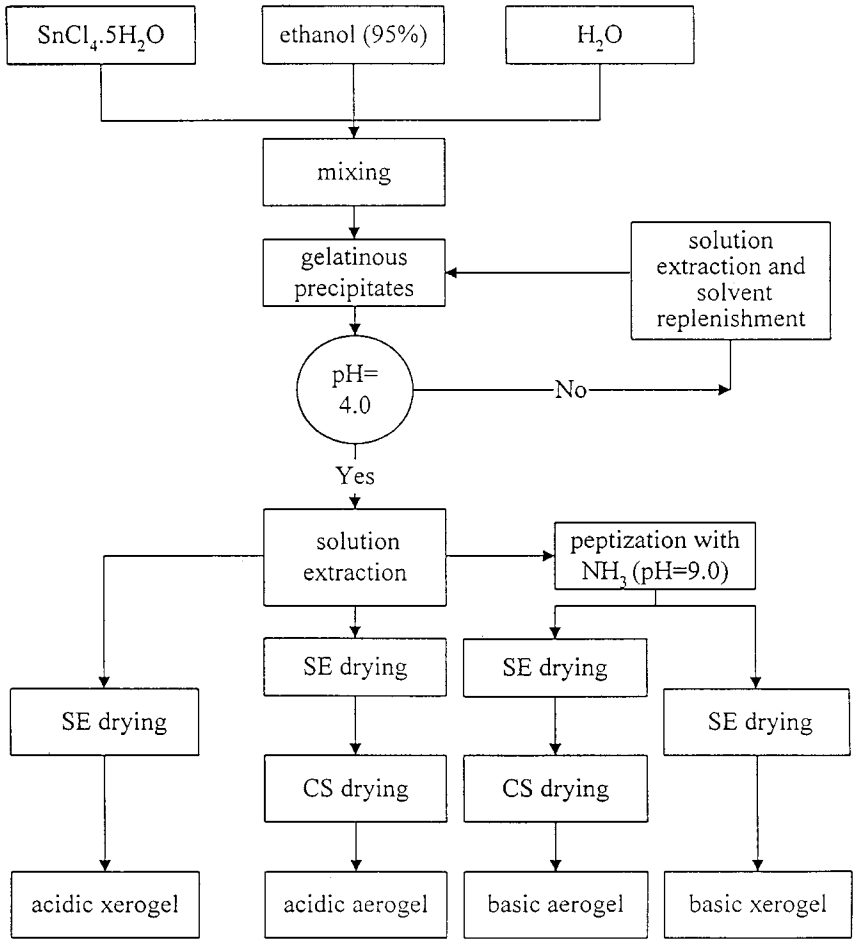

Figure 1 The preparative procedures of the tin oxide gels.

For CS drying, gels were first consecutively immersed in aqua-acetonic solutions with increasing acetone contents, ranging from 50% (by volume) to 100% with 10% increment between solutions for the first-step solvent-exchange. (The gradual increment in acetone concentration is to minimize cracking of the gel caused by surface tension.) The gels were then moved to a windowed autoclave, where the second solvent-exchanging step was carried out by continuously flushing the autoclave with flowing $CO_{2(l)}$ for ~0.5 h at 6.2 MPa. The final drying step was carried out by first raising the temperature to 40 °C and the pressure simultaneously went up to ~9.6 MPa. The entire system was then allowed to equilibrate for 0.5 h and finally vented. To facilitate discussion, the gels that were dried exclusively by the solvent-evaporation will be referred to as *xerogels*, while those by the hybrid processes as *aerogels* (because of their significantly greater pore volumes than the xerogels). At the end of the CS drying, the gels were placed inside a closed container with controlled humidity of ~30% at room temperature. Gels were found to continue to shrink within a period less than 8 h.

The microstructures of the dried gels were characterized by using nitrogen adsorption (ASAP2000, Micromeritics), scanning and transmission electron microscopies (SEM; Hitachi, S800; TEM; Hitachi, H7100). ζ (zeta)-potential was measured by using a ζ-potentiometer (Malvern, Zetamaster), while the size distributions of the wet gels and sols were determined by a Malvern 4700 C light-scattering particle-size analyzer.

3. Results and discussion

The sol used in preparing the basic gels contained particles having an average ζ-potential of -75 (± 3) mV and a size distribution that peaked at ~6 nm with 80% (by weight) having a size less than 20 nm [16]. The transparency exhibited by the sol indicated that the particles are well dispersed. On the other hand, no reproducible ζ-potential and particle size distribution data can be obtained from the acidic precipitate due to its instability against coagulation. In all measurements, however, the precipitate gave a negative potential with an absolute value less than 35 mV.

When dried exclusively by the SE process, both basic and acidic hydrous gels give transparent xerogels and their pore structures are extremely similar (Figs 2 and 3; Table I). Both xerogels contain predominantly micropores with a mean pore diameter of ~2.0 nm, a BET surface area of ~210 (± 10) m^2/g and a pore volume of ~0.1 cm^3/g at $P/P_0 = 0.9803$. TEM also indicated the presence of nanocrystallites in both xerogels, which have an average crystal size of ~2 nm and account for ~50% (in volume) of the skeleton [13].

The microstructures of the acidic and basic aerogels, on the other hand, are remarkably different until the gels have been subjected to the SE pre-drying to certain extent. Acidic aerogels with an SE-drying duration as

TABLE I Adsorption data of dried tin oxide gels

Sample[a]	SE drying[b] duration (h)	Apparent density[c] (g/cm^3)	BET surface area (m^2/g)	Pore volume, V_p^d (cm^3/g)	Macro-pore volume, V_{mp}^e (cm^3/g)
A-0	0	0.11	283	0.7	8.0
A-24	24	0.20	290	0.76	4.0
A-48	48	0.50	260	0.66	1.1
A-72	72	1.8	257	0.41	0.0
A-X	—	3.0	210	0.11	0.0
B-24	24	0.70	250	0.80	0.40
B-48	48	1.20	250	0.52	0.08
B-72	72	2.0	240	0.34	0.0
B-X	—	3.2	200	0.10	0.0

[a]A-: acidic gels; B-: basic gels; -X: xerogels. [b]The duration of solvent-evaporation (SE) drying prior to the CO_2 supercritical drying step. [c]The apparent density is determined directly from the weigth and dimension of the aerogel. [d]Single-point pore volume at $P/P_0 = 0.9803$. [e]The macropore volume, V_{mp}, is calculated based on a skelton density, ρ_{sk}, of 4.3 g/cm^3 and apparent density, ρ, by $V_{mp} = [(1/\rho) - (1/\rho_{sk})] - V_p$, where V_p is from column 5.

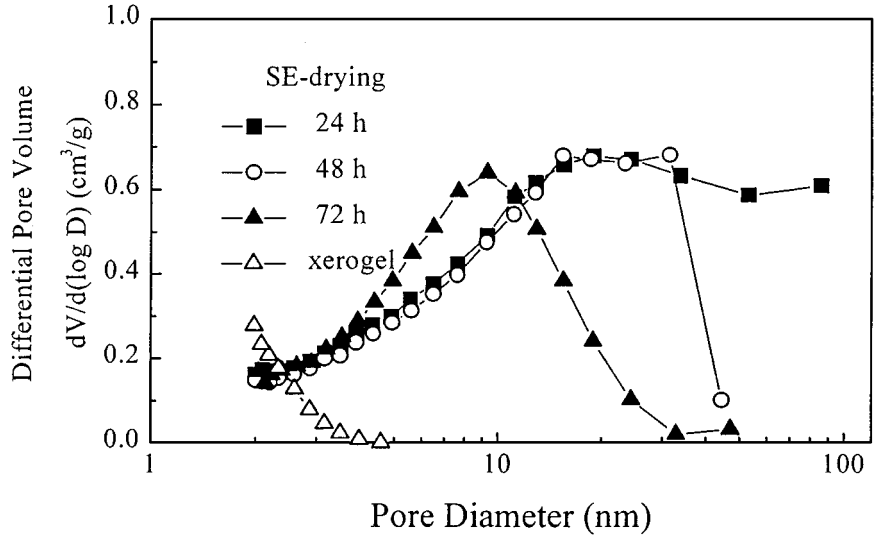

Figure 2 The BJH adsorption pore size distributions of the acidic aerogels and xerogel. SE-drying stands for the solvent-evaporation drying step conducted prior to CO_2 supercritical drying.

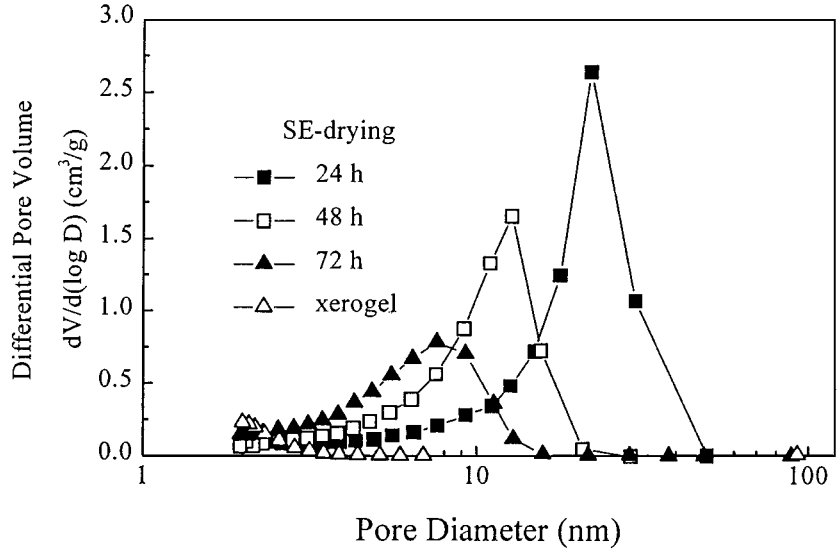

Figure 3 The BJH adsorption pore size distributions of the basic aerogels and xerogel. SE-drying stands for the solvent evaporation drying step conducted prior to CO_2 supercritical drying.

long as 48 h contain broccolilike oxide agglomerates and irregular voids having a characteristic dimension ranging from a few tenths to over 1 μm (Fig. 4a). The basic aerogel subjected to the same SE drying duration clearly has a much more compact structure, showing very small amount of rounded pores having a diameter of $\sim$0.1 μm (Fig. 4c). The microstructural difference diminishes with increasing SE-drying duration (Fig. 4b and d). The microscopic observations are consistent with the adsorption data.

For most of the aerogels, it was found that the pore volumes determined from the adsorption experiments

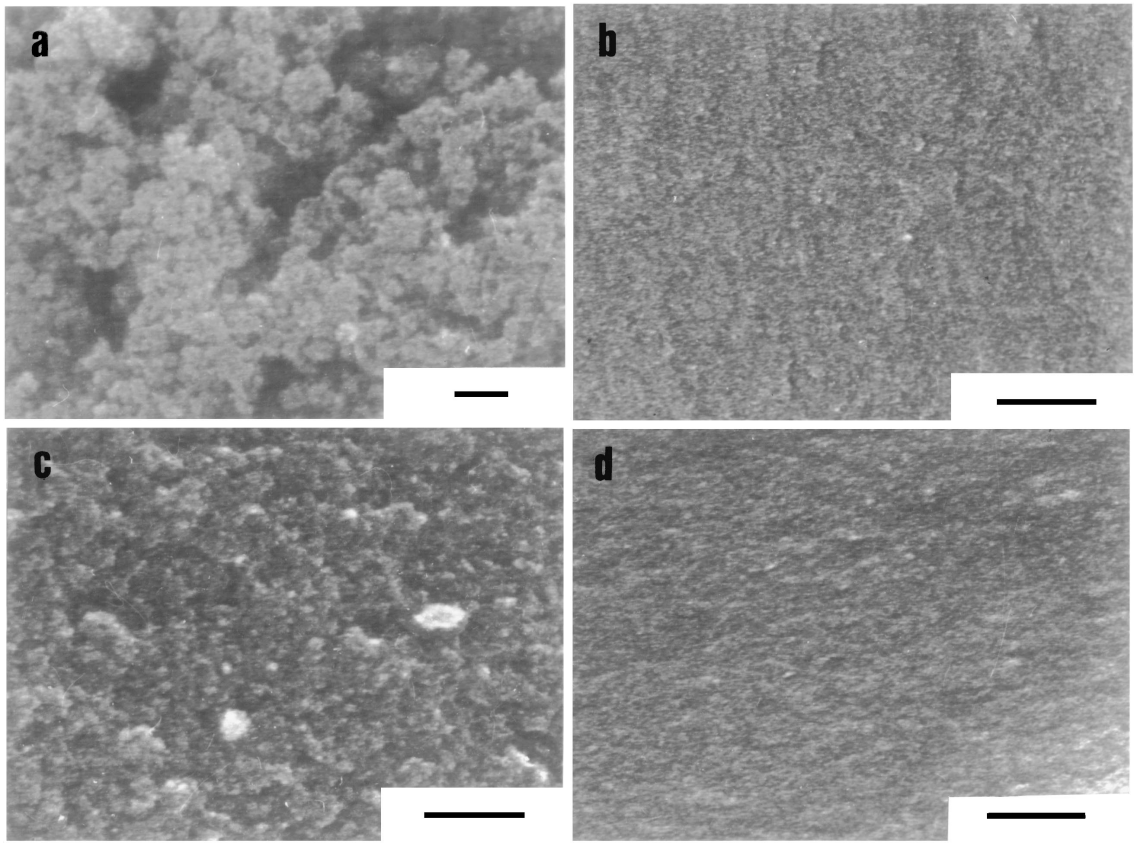

Figure 4 SEM micrographs of the fracture surfaces of the dried gels. Shown are: (a) acidic aerogel with an SE drying duration of 48 h; (b) acidic xerogel; (c) basic aerogel with an SE drying duration of 24 h; (d) basic xerogel. The scale bars correspond to a length of 0.3 μm.

are smaller than those deduced from their geometric densities. The inconsistency resides in the presence of the pores with a diameter greater than 0.1 μm (i.e., 100 nm), which can not be determined accurately by nitrogen adsorption. To facilitate comparison, the pores with a diameter greater than 100 nm will be referred to as macropores and their total volume, V_{mp}, is calculated from

$$V_{mp} = [(1/\rho) - (1/\rho_{sk})] - V_p$$

where ρ is the apparent density, ρ_{sk}, the skeleton density, and V_p, the total pore volume for pore diameters smaller than 100 nm (corresponding to $P/P_0 = 0.9803$), assuming that the aerogels have the same skeleton density ($\sim$4.3 g/cm^3) as the xerogel. This estimation is believed to be close to reality, since the very last shrinking step, i.e., the re-hydration step, is expected to enable condensation to proceed to approximately the same extent within the skeleton for both aero- and xero-gels. Fig. 5 compares V_{mp} and V_p for differently dried gels. Both the pore-size distribution (PSD; Figs 2 and 3) and pore volume (Fig. 5) data indicate that, with an SE drying duration up to 48 h, the acidic aerogels have a much greater macropore volume

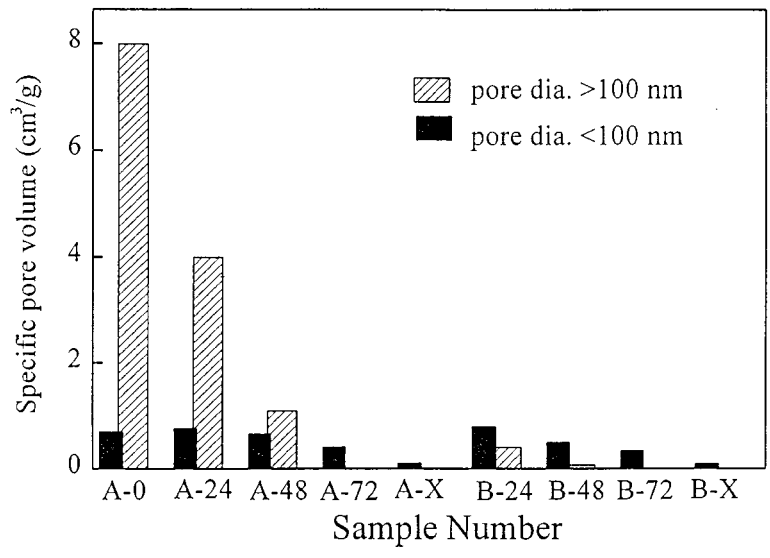

Figure 5 The effect of drying protocol on pore volume distribution. A- and B- stand for acidic and basic gels, respectively and the numbers that follow indicate the duration of the solvent evaporation step (in hour). -X stands for xerogel.

and broader PSD than the basic ones. Macropores prevail in all these acidic aerogels, while they account for less than one half of the total pore volume in the basic aerogel having an SE duration as short as 24 h.

Although both aerogels showed a decrease in pore size with increasing SE drying duration, their PSDs in the mesopore (pores with a diameter between 2 and 100 nm) region varied in different manners. That is, with increasing SE-drying duration, the PSD of the acidic aerogel showed decreasing intensity at the large-pore front but with the small-pore tail being almost intact. Overall, the PSD becomes increasingly narrowed with the extent of the SE drying. The PSD of the basic aerogel, on the other hand, remains sharp and progressively shifts toward smaller pore sizes. The differences in pore volume and PSD between the acidic and basic aerogels can be reasoned in terms of their wet-gel structures and mechanisms causing pore contraction during each of the drying steps, as discussed below.

The basic sol contains particles having similar sizes and high surface potentials. Balancing in electrostatic forces is expected to enable the particles to arrange themselves with similar distances from one another, resulting in a narrow PSD. On the other hand, the acidic gel, owing to its low surface potential, contains coagulated masses and is expected to contain widely distributed pore sizes with smaller pores within the masses and large ones between them.

The gel shrinkage, and hence pore contraction, during SE drying is known to arise from capillary force exerted at the liquid-vapor interface. Pore contracts in order to compensate the loss of solvent inside the pore. Because the solvent (i.e., water) in larger pores has a higher vapor pressure, they empty and hence contract earlier than the smaller ones. This results in the preferential loss in the large pores with increasing extent of SE drying, as observed for the acidic aerogels (Fig. 2). For the basic gels, the pores have similar diameters and thus response, i.e., contract, at similar rates. As a result, the uniformity in PSD is mostly retained during SE drying (Fig. 3).

Macroscopically, the partially dried basic and acidic gels with an SE-drying duration up to 48 h have been known to exhibit very different gel-shrinking behaviors during the solvent-exchanging steps in CS drying [16]. The basic gels shrank primarily ($\geq$70% of the overall shrinkage during the entire CS drying process) during the first solvent-exchanging step. The shrinkage is correlated with the reduction in ζ-potential, which in turn is due to a decrease in solvent dielectric constant [16]. When the basic sol was dispersed in the acetone/water mixtures, for example, $|\zeta$-potential| was found to first gradually decrease from $\sim$75 to $\sim$60 mV with an acetone/water (by volume) ratio increasing up to 90/10 and then rapidly drop to 35 mV in pure acetone. That is, during most of the solvent-exchanging period, the particles retained a fairly high surface potential, which is expected to allow the particles to homogeneously slide against one another. The narrowness in PSD is hence mostly preserved.

On the other hand, the acidic gels shrank only during the second step and the shrinkage is due to the osmotic compressive pressure that arises from an increase in the liquid-solid (gel skeleton) interfacial energy with increasing CO_2 concentration [16]. By this mechanism, the smaller pores, which have a higher surface-to-volume ratio, are expected to contract first, causing a greater shrinkage within the coagulated masses than between the masses and leaving large voids (macropores) preferentially between the masses. Thus, unlike the SE drying process, pore contraction during this step does not help to narrow the pore-size variation within the acidic gels.

For both acidic and basic gels with an SE-drying duration of 72 h, no shrinkage took place during CS drying. Clearly, the gel structures became stiff enough to resist the contraction forces operative during the CS drying process. Consequently, the pore structures of these aerogels are not affected by the CS drying process.

At the end of the CS step, no further shrinkage took place if the aerogels were not exposed to the ambient by, for example, either leaving the gels in the autoclave chamber or quickly transferring them to an evacuated chamber. On the other hand, aerogels shrank when they were exposed to an environment containing water vapor and the shrinking rate was found to increase with humidity. These results indicate that water plays an important role for the shrinkage. The CS-dried aerogels are known to be hydrophilic in nature [15] and water vapor either adsorbs onto the gel skeleton or condenses to fill up part, if not all, of the pores. The effects of water on the shrinkage could be either chemical or physical. For the former, absorption of water re-activates the condensation reaction between hydroxyl surface groups, while for the latter, pore contracts because of the capillary-force effect.

Fig. 6 compares the PSDs of the aerogels that are measured either immediately after the CS step or after the shrinkage completely ceased at room temperature in the humid environment. As shown, the effects of this re-hydration step on PSD are very similar to the SE drying step. Namely, for the acidic aerogels, it causes a preferential decrease in the large-pore intensity, leading to narrowing in PSD. Such variation is due to the fact that the solid skeleton surrounding larger pores is less compact than that surrounding the smaller ones and hence is expected to be less resistant to contraction. For basic gels, on the other hand, the shrinkage causes shift in peak profile toward smaller pore sizes without significant change in distribution width.

In summary, hydrous tin oxide gels having different surface potentials have been subjected to an SE + CS drying protocol, followed by re-hydration at low humidity. In principle, the width of PSD and total pore volume are simultaneously affected by the magnitude of the particle surface potential and the duration of the SE drying, while the mean pore size can be controlled by the latter. Accordingly, varieties of pore structures have been obtained by varying these two parameters.

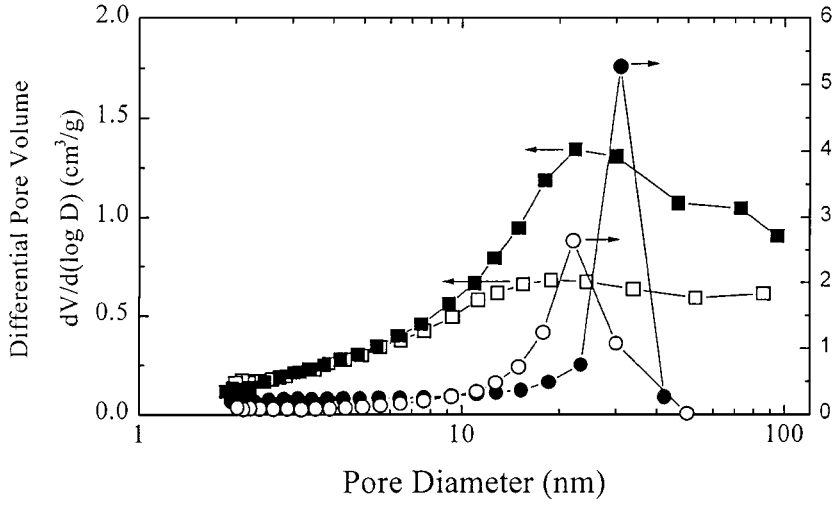

Figure 6 The BJH adsorption pore size distributions of the acidic (square symbols) and basic (circle) aerogels either with (open symbols) or without (solid) being subjected to re-hydration at 30% humidity after CO_2 supercritical drying.

Acknowledgement

This work is supported by the National Science Council of Republic of China under contract number of NSC84-2216-E-002-020.

References

1. M. J. FULLER and M. E. WARWICK, *J. Catal.* **29** (1973) 441.
2. F. SALA and F. TRIFIRO, *ibid.* **34** (1974) 68.
3. P. G. HARRISON and P. J. F. HARRIS, U.S. Patent 5,051,393 (1991).
4. T. SEIYAMA, A. KATO, K. FUJISHI, and M. NAGATANI, *Anal. Chem.* **34** (1962) 1502.
5. K. TAKAHATA, in "Chemical Sensor Technology," Vol. 1, edited by T. Seiyama (Kodansha, Tokyo, and Elsevier, Amsterdam, 1988) p. 39.
6. A. CAMANZI and G. SBERVEGLIERRI, U.S. Patent 5, 185,130 (1993).
7. T. J. COUTTS, in "Active and Passive Thin Film Devices" (Academic Press, London, 1978).
8. J. C. MANIFACIER, *Thin Solid Films* **90** (1982) 297.
9. J. F. GOODMAN and S. J. GREGG, *J. Chem. Soc.* **237** (1960) 1162.
10. R. S. HIRATSUKA, S. H. PULCINELLI and C. V. SANTILLI, *J. Non-Cryst. Solids* **121** (1990) 76.
11. K. L. CHOPRA, S. MAJOR and D. K. PANDYA, *Thin Solid Films* **102** (1983) 1.
12. N. L. WU, L. F. WU, Y. C. YANG and S. J. HUANG, *J. Mater. Res.* **11** (1996) 813.
13. N. L. WU, L. F. WU, I. A. RUSAKOVA, A. HAMED and A. P. LITVINCHUK, *J. Amer. Ceram. Soc.* (1998), in press.
14. Y. KOBAYASHI, M. OKAMOTO and A. TOMITA, *J. Mater. Sci.* **31** (1996) 6125.
15. C. J. BRINKER and G. W. SCHERER, "Sol-Gel Science" (Academic Press, 1990).
16. S. Y. WANG and N. L. WU, *J. Non-Cryst. Solids* **224** (1998) 259.

Received 7 July
and accepted 23 December 1998